International Journal of Nanomedicine

Dovepress
open access to scientific and medical research

Open Access Full Text Article

ORIGINAL RESEARCH

Improving ^{131}I Radioiodine Therapy By Hybrid Polymer-Grafted Gold Nanoparticles

This article was published in the following Dove Press journal:
International Journal of Nanomedicine

Marine Le Goas[1]
Marie Paquet[2–5]
Aurélie Paquirissamy[1]
Julien Guglielmi[2–4]
Cathy Compin[2–4]
Juliette Thariat[6]
Georges Vassaux[2–4]
Valérie Geertsen[1]
Olivier Humbert[2–5]
Jean-Philippe Renault[1]
Géraldine Carrot[1]
Thierry Pourcher[2–4]
Béatrice Cambien[2–4]

[1]NIMBE, Commissariat à l'Energie Atomique, Centre National Recherche Scientifique UMR 3685, Université Paris-Saclay, Gif-sur-Yvette, France; [2]Laboratory Transporter in Imaging and Radiotherapy in Oncology (TIRO), Institut de Biosciences et Biotechnologies d'Aix-Marseille (BIAM), Commissariat à l'Energie Atomique, Nice, France; [3]Laboratory Transporter in Imaging and Radiotherapy in Oncology (TIRO), University Nice Sophia Antipolis, Nice, France; [4]Laboratory Transporter in Imaging and Radiotherapy in Oncology (TIRO), University Côte d'Azur, Nice, France; [5]Nuclear Medicine Department, Centre Antoine Lacassagne, Nice, France; [6]Department of Radiation Oncology, Centre François Baclesse, Université de Normandie, Caen, France

Correspondence: Béatrice Cambien
Laboratory Transporter in Imaging and Radiotherapy in Oncology (TIRO), University Nice Sophia Antipolis, 28 Avenue Valombrose, Nice Cedex 2 06107, France
Tel +33 493 377 715
Email cambien@unice.fr

Background: Human trials combining external radiotherapy (RT) and metallic nanoparticles are currently underway in cancer patients. For internal RT, in which a radioisotope such as radioiodine is systemically administered into patients, there is also a need for enhancing treatment efficacy, decreasing radiation-induced side effects and overcoming radio-resistance. However, if strategies vectorising radioiodine through nanocarriers have been documented, sensitizing the neoplasm through the use of nanotherapeutics easily translatable to the clinic in combination with the standard systemic radioiodine treatment has not been assessed yet.

Method and materials: The present study explored the potential of hybrid poly (methacrylic acid)-grafted gold nanoparticles to improve the performances of systemic ^{131}I-mediated RT on cancer cells and in tumor-bearing mice. Such nanoparticles were chosen based on their ability previously described by our group to safely withstand irradiation doses while exhibiting good biocompatibility and enhanced cellular uptake.

Results: In vitro clonogenic assays performed on melanoma and colorectal cancer cells showed that poly(methacrylic acid)-grafted gold nanoparticles (PMAA-AuNPs) could efficiently lead to a marked tumor cell mortality when combined to a low activity of radioiodine, which alone appeared to be essentially ineffective on tumor cells. In vivo, tumor enrichment with PMAA-AuNPs significantly enhanced the killing potential of a systemic radioiodine treatment.

Conclusion: This is the first report of a simple and reliable nanomedicine-based approach to reduce the dose of radioiodine required to reach curability. In addition, these results open up novel perspectives for using high-Z metallic NPs in additional molecular radiation therapy demonstrating heterogeneous dose distributions.

Keywords: internal radioisotope therapy, radioiodine, polymer-grafted gold nanoparticles, melanoma, colorectal cancer, radio-enhancement

Introduction

Radiotherapy (RT) has been widely used for cancer treatment. Apart from external beam radiotherapy (EBRT) with radiation beams applied onto tumors externally, internal radioisotope therapy (RIT) is another important modality of cancer therapy carried out either by the in situ implantation of radioactive sources or by their systemic administration to irradiate tumors from inside the body. However, there are numerous situations in which dose delivery is limited by the tolerance of surrounding normal tissues. Moreover, resistance often occurs during RT, especially for tumors after multiple rounds of treatment, as well as tumors with high levels of hypoxia as oxygen is required to enhance cell DNA damage caused by ionizing radiation in RT.[1] Enhancement strategies have been proposed and include a combination of RT with other therapeutic approaches such as chemotherapy,[2] oncolytic viruses[3] or

submit your manuscript | www.dovepress.com
DovePress
http://doi.org/10.2147/IJN.S211496

radiosensitizing pharmacological agents which interfere with DNA repair and increase cytotoxicity (such as ataxia-telangiectasia mutated,[4] poly-(ADP-ribose)-polymerase[5] or DNA-dependent protein kinase (DNA-PK) inhibitors[6]). Recently, with the advances in nanotechnology, a new strategy involving metal-containing nanoparticles has been proposed to enhance the sensitivity of tumors to EBRT through the production by the metal of additional low-energy secondary electrons and of reactive oxygen species.[7–11] Following convincing pre-clinical evidences, clinical trials combining EBRT and metallic nanoparticles are currently underway to assess the efficacy of the approach in patients affected with different types of cancers.[12–14]

For RIT in which a radioisotope is systemically administered into patients, the nanotherapeutics-based development to enhance cancer therapy has not entered human trials yet. In RIT, one of the frequently used radioisotopes is ^{131}I, either administered alone into the bloodstream or linked to antibodies targeting specific markers expressed at the surface of cancer cells.[15] The second option intends to target and treat tumors that do not naturally uptake radioiodine. In contrast, the first option selectively targets the cancer cells that express the Na/I symporter (NIS) either endogenously such as differentiated thyroid carcinoma[16] or ectopically in the case of gene therapy-mediated RIT.[17] For thyroid cancer, however, resistance to repetitive treatment and radioiodine-refractory thyroid cancers are currently the major causes of deaths related to thyroid cancer and do not have effective treatments.[18] In addition, the applicability of radioiodine to treat non-thyroidal neoplasms is still hampered by the reduced capacity of such tumors to accumulate ^{131}I.[19,20] Therefore, new strategies are currently investigated by our group and others in order to improve ^{131}I efficacy.[21,22] In this context, sensitizing the neoplasms through the use of nano-agents easily translatable to the clinic in combination with the standard systemic radioiodine treatment may offer a new opportunity to improve ^{131}I-based strategies and overcome radioiodine refractoriness.

So far, only a few nanotherapeutics-based approaches have been developed in combination with radioiodine. Their purposes were either to enhance the targeting ability of radioiodine using non-metallic nanoparticles[23] or to improve radioiodine efficacy through combination with other drugs.[24,25] Besides radioiodine, metallic nano-particles conjugated to radioisotopes (^{211}At, ^{99m}Tc, Rhenium 188,[26–29]) sharing with iodine the property to be strongly adsorbed on gold or silver metal surface have demonstrated a successful radio-enhancing potential. Although very innovative in formulation design, such strategies may have the major inconvenient to modify the properties of the radiopharmaceutical, in particular its ability to be taken up by the thyroid. In addition, minimizing the complexity of nanotherapeutics for human use may markedly improve their potential to be translated into a clinically applicable therapeutic.[30] As a consequence, radiolabeled nanomaterials are not clinically translatable to treat thyroid cancer.

Therefore, there is a need for therapeutically enhanced strategies combining the action of clinically translatable metallic nanoparticles to that of systemic ^{131}I treatment, given separately. While studies in cell culture models have shown gold nanoparticles radiosensitization in the context of brachytherapy using I-125 seeds,[31] no study has provided experimental in vivo evidence of AuNP radio-enhancement potential during systemic ^{131}I-based therapy such as routinely performed in clinical practice.

o address this question, gold nanoparticles were chosen based on their good safety profile, their ability to strongly interact with incident radiation then to increase the dose deposited close to the nano-object. Because nanoparticles are usually difficult to handle, due to their tendency to aggregate and even precipitate in biological fluids and analogues,[32] we synthesized polymer-grafted nanoparticles, to ensure good dispersibility and long-term stability in biological media. These polymer-grafted gold nanoparticles were prepared in one step, via a direct method using polymer ligands obtained by controlled radical polymerization[33] and previously proved to ensure nanoparticle biocompatibility and enhanced cellular uptake.[34] The behavior of the synthesized nano-objects has been extensively characterized before and under irradiation.[33] It was particularly shown that PMAA-AuNPs can safely withstand doses higher than 300 Gy, which is the maximum dose achieved in radioiodine treatment.[35]

The present study assessed the use of PMAA-AuNPs for the radio-enhancement of ^{131}I-mediated RIT both on tumor cells and on murine tumors and provided the proof-of-concept that combination therapy helps reduce the dose required to reach curability. To the best of our knowledge, this is the first report of a simple and reliable nanomedicine-based approach to enhance the therapeutic efficacy of standard radioiodine treatment using biocompatible PMAA-AuNPs and showing substantial potential for clinical translation.

Materials And Methods

Preparation Of PMAA-Grafted Gold Nanoparticles (PMAA-AuNPs)

The synthesis was performed elsewhere.[33] Briefly, poly (tert-butyl methacrylate) (PMAtBu) ligands were first obtained through an atom-transfer radical polymerization with bis [2-(2-bromoisobutyryloxy)ethyl] disulfide and $Cu^{I}Br$/pentamethyldiethylenetriamine (PMDETA), respectively acting as initiator and catalytic system. The $Cu^{I}Br$/PMDETA/initiator ratio was 2/2/1. The reaction was performed during 5 hrs in DMF at 60°C, under argon atmosphere. The polymer was subsequently precipitated and filtrated. PMAtBu was then hydrolyzed into PMAA, through the action of trifluoroacetic acid in chloroform. Gold nanoparticles were obtained via the reduction of $HAuCl_4$ by $NaBH_4$ in methanol, in the presence of disulfide-PMAA, which acted as ligands (Figure 1A). The resulting PMAA-AuNPs were collected by centrifugation, washed and dried under nitrogen. The nano-objects are composed of a gold core with a diameter of 3 nm, and a 10 nm-thick polymer corona, as measured from scattering techniques (Table 1).[33]

Cryo-TEM Observations

Three microliters of a 5 mg/mL nanoparticles solution was applied to a Lacey carbon-coated copper grid. After 1-min incubation, the excess of liquid was removed by blotting with filter paper and the grid rapidly plunged into liquid ethane. Analyses were carried out on a JEOL-1400 instrument operated at 120 kV at cryogenic temperature.

Stability Of PMAA-AuNPs In Aqueous Solutions

UV-visible spectroscopy was used to study the stability of PMAA-AuNPs in four aqueous solutions: pure water, Dulbecco's Phosphate-Buffered Saline (DPBS), pure DMEMand DMEM supplemented with 10% FCS (fetal bovine serum). Solutions were prepared at 0.14 mg/mL of NPs. Solutions in pure DMEM and supplemented DMEM were measured again after a 7-day incubation. All absorption spectra were recorded using a Shimadzu UV-2450 double-beam UV−Vis spectrophotometer.

Cell Culture

The B16F10 melanoma cells (obtained from ATCC) and the DHD/K12/TRb colorectal cancer cells (obtained from

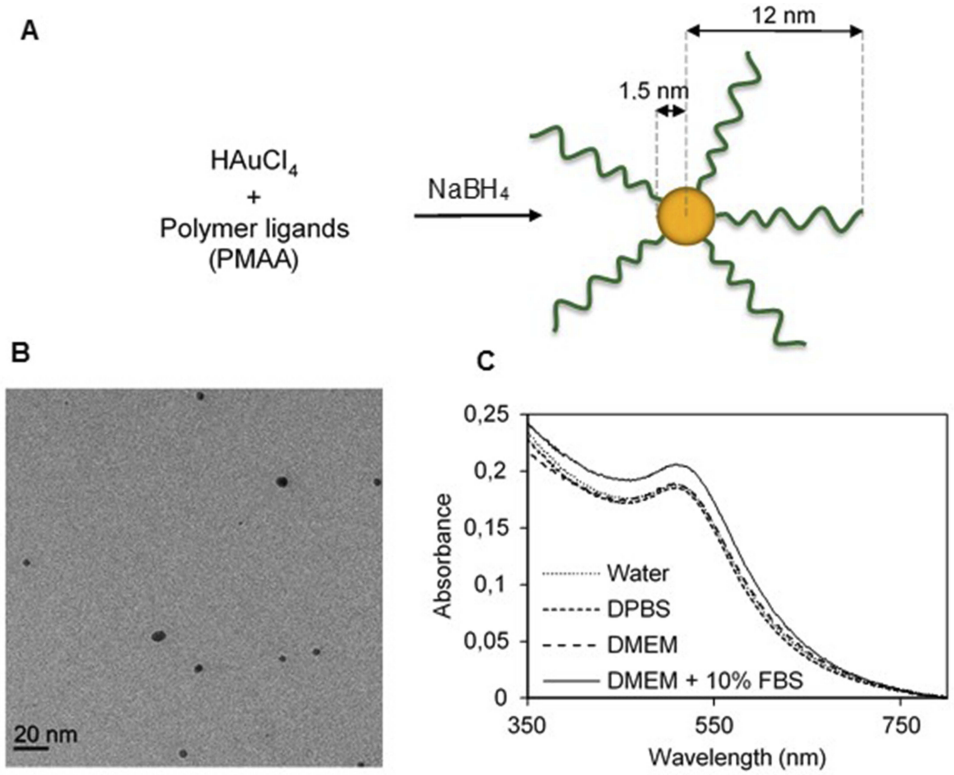

Figure 1 Synthesis and characterization of PMAA-AuNPs. (**A**) Scheme of the direct synthesis of PMAA-AuNPs. (**B**) Cryo-TEM image of the obtained NPs. (**C**) UV-vis spectra of PMAA-AuNPs in various aqueous solvents (water, DPBS, DMEM, DMEM+10% FBS).

Table 1 Summarized Characteristics Of PMAA-AuNPs

Characteristics	PMAA-AuNPs
M_n of polymer chains	4,600 g/mol
Gold core radius obtained by SAXS	1.5±0.7 nm
$\%_{wt}$ organic content	71%
Nano-object radius obtained by SANS[33]	12.0±0.3 nm
Grafted chains density	4.6±0.2 chains/NP
Zeta potential in phosphate buffer pH 7.5	− 40 mV±8 mV

Sigma) were cultured in DMEM (GIBCO, France) supplemented with 10% heat-inactivated fetal calf serum (FCS, GIBCO) at 37°C under a humidified atmosphere containing 5% CO_2. Cells were passaged by using 0.05% trypsin. Both cell lines were transfected with pcDNA3.1-mNIS (murine NIS)[36] using the FuGENE 6 reagent (Roche) according to the manufacturer's instructions. Stable clones were selected by addition of 1 mg/mL geneticin (G418) to the medium 3 days after transfection. One clone with high functional expression of NIS was selected for each cell line.[37]

Immuno-Fluorescence Experiments

NIS-B16F10 cells plated in 24-well format were allowed to grow 24 hrs at 37°C and 5 % CO_2 before being fixed (2% PFA) and permeabilized (0.1% triton). After a blockade step (BSA 1%), immunofluorescence labelling was performed according to[38] using NIS Ab25, anti-mNIS is an affinity purified rabbit polyclonal antibody as previously described.[39]

Iodide Uptake

Iodide uptake in whole cells was performed according to[38] with 30 µM NaI and ^{125}I. Measurements were made after 1 hr in the presence or the absence of 100 mM perchlorate, a NIS inhibitor. The radioactivity was measured using a gamma counter (Packard Cobra).

ICP-MS Analysis

PMAA-AuNPs cellular uptakes of both DHD-NIS and B16-NIS were determined by inductively coupled plasma mass spectrometry (ICP-MS). The samples were prepared as follows: 350,000 cells were plated in a 6-well format. After 24 hrs, the culture medium was replaced with 2 mL of fresh medium containing 0, 0.02 or 0.2 mg/mL PMAA-AuNPs and the cells were incubated during 24 hrs at 37°C. Non-internalized NPs were removed by 3 successive washings with 1× DPBS (pH 7.4). Cells were trypsinized and isolated by centrifugation. Cell pellets were sonicated during 30 mins before an overnight digestion under stirring with 100 µL aqua regia at 70°C to dissolve the nanoparticles and mineralize the cells. After a second sonication for 30 mins, samples were diluted with 2% HCl and filtered through a 0.45 µm PTFE membrane. The gold concentrations were determined by ICP-MS (iCAP Q Thermo Electron) after external calibration by dilutions of a certified gold solution (SPEX,-CertiPrep). Measurements were repeated three times before averaging. All dilutions (samples and standards) were prepared by weight.

Clonogenic Cell Survival Assay

The radio-enhancement potential of PMAA-AuNPs to DHD-NIS and to B16-NIS cells was assessed using clonogenic assays. Different number of cells (100, 300, 1000, 5000, 10,000) were plated in 12-well format. After 24 hrs, the culture medium was replaced with 1 mL of fresh medium or medium containing PMAA-AuNPs nanoparticles at the indicated concentrations and incubated for 2 hrs at 37°C. After 3 washes with 1× PBS (pH 7.4), the treated cells were exposed for 4 hrs to 0, 0.04, 0.2, 0.7, 1.8, 5.5 or 11 MBq of ^{131}I (IBA, France) before being cultured for 9–14 days. The colonies were fixed with methanol and stained with 0.4% crystal violet. Finally, the plates were inspected by microscopy and the number of the colonies (at least 50 cells) was counted. Each assay was made in triplicate.

Mice

Eight-week-old Balb/c female athymic (nude) mice were obtained from Janvier (Le Genest Saint Isle, France). Animal housing and procedures were conducted according to French Agriculture Ministry guidelines and were approved by the CIEPAL-Azur local ethics committee.

In Vivo microSPECT/CT Studies

SPECT/CT imaging analysis was performed as previously described.[21,40] Briefly, ^{99m}Tc pertechnetate ($^{99m}TcO_4^-$) was obtained from a freshly eluted $^{99}Mo/^{99m}Tc$ generator. Animals were administered activities of 15 MBq $^{99m}TcO_4^-$ intraperitoneally (i.p.). Tracer uptake was measured at different times using a dedicated microSPECT/CT scanner (eXplore speCZT CT120, GE) under gas anesthesia (air and 1–2% isoflurane) in an air-warmed imaging chamber (Minerve, Esternay, France) to maintain body temperature at 37°C. The SPECT scanner uses a stationary full ring of CZT detectors and a rotating 7-pinhole (1 mm opening)

collimator. A total of 350 projections were acquired over 360° in 8 mins. Images were reconstructed using the manufacturer's 3D-OSEM algorithm (5 subsets and 11 iterations), which incorporates the system's collimator–detector response function and scatter correction. Reconstructed images were analyzed and quantified using AMIDE software.[41]

Tumor Treatments

Briefly, each mouse was subcutaneously injected with 1×10^6 B16-NIS cells in the flank. An apparently visible tumor mass was observed 4 days after injection. At day 6, when the tumor size averaged 100 mm^3, the mice were randomly divided into four groups: control group (saline only), PMAA-AuNPs group, ^{131}I group, and PMAA-AuNPs/^{131}I group. Five mice were included in each group. Mice treated with nanoparticles received three intratumoral injections of PMAA-AuNPs (1 mg/mL [Au]) on day 6 and mice of ^{131}I groups were injected i.p. with 22 MBq on day 7. Mice were monitored after drug treatments. The longest (a) and shortest (b) tumor diameters (mm) were recorded and formula for an ellipsoid sphere ($0.52\times a\times b^2$) was utilized to determine the volume of tumor. Tumors were preserved in liquid nitrogen for future studies.

Histology/Immunohistochemistry

Formalin-fixed, paraffin-embedded tumor sections were stained with hematoxylin/eosin for morphologic evaluation. The sections were analyzed by a certified veterinary pathologist. The numbers of necrotic cells were assessed by three independent evaluations.

Statistical Analysis

Statistical analysis was performed using Prism (GraphPad software). Dual comparisons were made using a Student's *t*-test and comparisons between multiple conditions were analyzed using ANOVA. Statistical significance was set at $p<0.05$.

Results

Synthesis And Characterization Of PMAA-AuNPs Nanoparticles

The polymer-grafted gold nanoparticles used for the present study were synthesized via a direct synthesis using polymer ligands, as described in a previous paper.[33] Briefly, gold salts were reduced in the presence of previously prepared disulfide-functional PMAA (polymethacrylic acid) which acted as ligands (Figure 1A), resulting in the formation of 3 nm AuNPs with grafted polymer chains onto the surface. The size of the AuNPs is controlled by the ratio ligands/gold salts, as previously described.[42] Detailed characterization of the resulting nano-objects was performed using various techniques[33] and main results are summarized in Table 1. Due to the presence of the polymer corona, the resulting nano-objects were non-aggregated in water, as shown by cryoTEM picture (Figure 1B).

Their stability in various aqueous solutions was studied through UV-visible spectroscopy. Indeed, the localization of the plasmon peak of AuNPs is highly dependent on their aggregation state.[43] Four solutions with increasing complexity were tested: pure water, DPBS, pure DMEM, and DMEM supplemented with 10% serum. We did not test 100% serum as our objects were not planned to be intravenously injected. No plasmon shift was observed for any solution (Figure 1C), proving the great stability of our PMAA-AuNPs, even when exposed to high salt and proteins concentrations. Small-angle X-ray scattering (SAXS) experiments confirmed this result (Figure S1). Stability was also preserved after extended periods of incubation (Figure S1).

Expression Of mNIS In B16F10 And DHD Cells And Ability To Uptake Iodine

mNIS cDNA was stably transfected in B16F10 melanoma and DHD colorectal cancer cells. The expression of NIS at the cell surface was visualized by immunofluorescence on both cell lines, B16-NIS are shown as an example (Figure 2A). The functional activity of the NIS symporter in both cell lines was analyzed by measuring iodide uptake. B16-NIS or DHD-NIS cells were incubated with ^{125}I in the presence of either saline buffer or perchlorate ($NaClO_4$), a specific NIS inhibitor. After 1 hr, cells were washed and cellular ^{125}I content was determined. Both cell lines were able to accumulate ^{125}I, in a NIS-dependent manner as indicated by the inhibition with perchlorate (Figure 2B).

Radiosensitivity Of B16-NIS And DHD-NIS To Radioiodine

We next evaluated the radiosensitivity of each cell line to ^{131}I in clonogenic cell survival assays. B16-NIS and DHD-NIS were exposed for 4 hrs to various activities of ^{131}I (ranging from 0 to 11 MBq), in the presence or the absence of perchlorate before being cultured for 9–14 days. The 50% lethal dose was reached with 0.45 MBq for DHD-NIS cells (Figure 2C) and with 0.66 MBq for

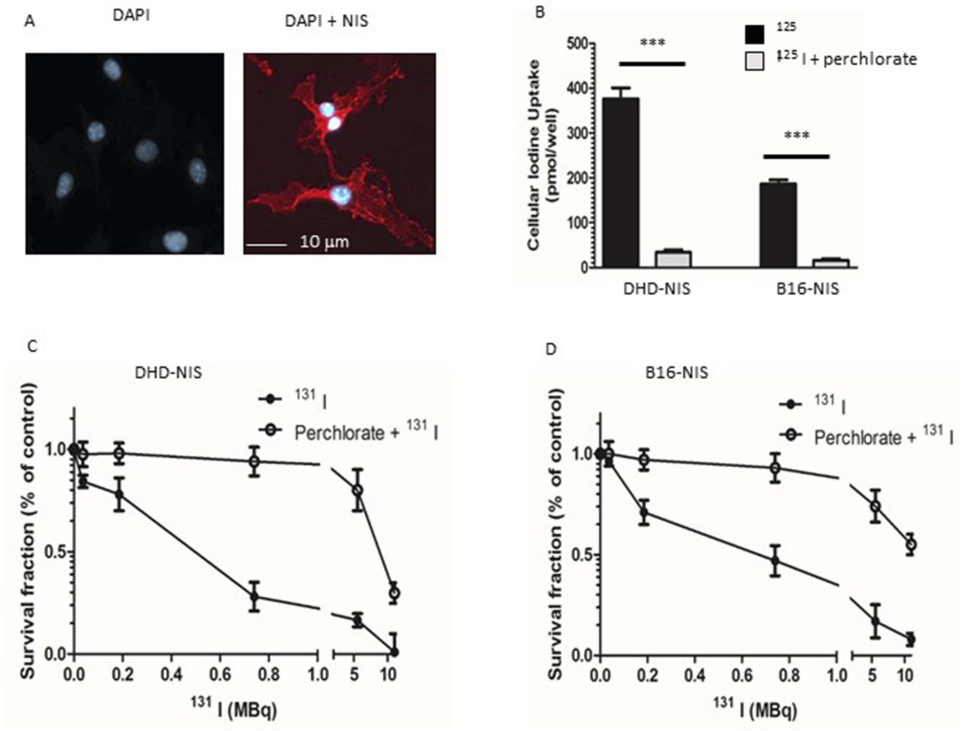

Figure 2 Sensitivity of NIS-expressing-B16 melanoma and -DHD colorectal carcinoma cells to radioiodine. (**A**) Immunofluorescence analysis of NIS expression in stably transfected B16-NIS cells. The expression of NIS at the cell surface was evaluated by using a specific anti-mouse NIS polyclonal antibody (right panel) or rabbit IgG (left panel). (**B**) Cellular iodine uptake by the DHD-NIS and the B16-NIS tumor cells. DHD-NIS or B16-NIS cells were incubated for 1 hr with ^{125}I in the presence or the absence of sodium perchlorate, a specific NIS inhibitor before being washed and lysed. Aliquots of lysates were counted in a γ counter. The data presented are the mean±standard error of the mean (SEM) of triplicates and are representative of three independent experiments. Radiation cell survival curves for DHD-NIS cells (**C**) and for B16-NIS cells (**D**). Clonogenic assays were performed on DHD-NIS or B16-NIS cells after treatment with ^{131}I alone (0 to 11 MBq for 4 hrs) or with a combination of sodium perchlorate and ^{131}I. ***p<0.001.

B16-NIS cells (Figure 2D), both being protected from radiation in the presence of perchlorate.

In Vitro Cytotoxicity And Cellular Uptake Of PMAA-Grafted Gold Nanoparticles (PMAA-AuNPs)

Studies were carried out with B16-NIS and DHD-NIS to determine the cytotoxicity of PMAA-AuNPs in clonogenic assays. Figure 3A and B shows the fraction of the viable cells after exposure for 2 hrs to several doses of nano-objects followed by cell culture for 9 to 14 days. A significant reduction in cell viability was observed when both cell types were incubated with nanoparticle concentrations reaching 250 µg/mL [Au]. In contrast, no significant cytotoxic effect of PMAA-AuNPs on the cell survival fraction was measured with concentrations in the range of 2.5 to 25 µg/mL [Au].

For quantification of nanoparticles taken up by DHD-NIS and B16-NIS cells, cells were collected after 24-hr incubations with non-toxic concentrations of PMAA-AuNPs (Figure 3C). Concentrations of Au in cell lysates were determined by ICP-MS and corresponding numbers of internalized AuNPs per cell were then estimated considering the size of the gold cores previously determined by SAXS (3 nm). Detectable levels of Au were measured in both cell types after exposure to low concentrations of PMAA-AuNPs (2.5 µg/mL [Au]). In addition, a ten-fold increase in the concentration of PMAA-AuNPs treatment led to a 2.3 and a 2.1-fold increase in the cellular uptake by the B16-NIS and the DHD-NIS, respectively, suggesting that the internalization process does not vary in proportion to the nanoparticle concentration. Upon exposure to 2.5 µg/mL as well as to 25 µg/mL [Au], higher masses of gold were detected in DHD-NIS cells compared to B16-NIS (320,000 vs 180,000, $p<0.05$, respectively).

Radiosensitizing Potential Of PMAA-AuNPs To ^{131}I On B16-NIS And DHD-NIS Cells

In order to determine whether PMAA-AuNPs could enhance the sensitivity of melanoma and colorectal cancer cells to radioiodine, the low ^{131}I activities of 0.1 and 0.2 MBq were, respectively, chosen for DHD-NIS and B16-NIS.

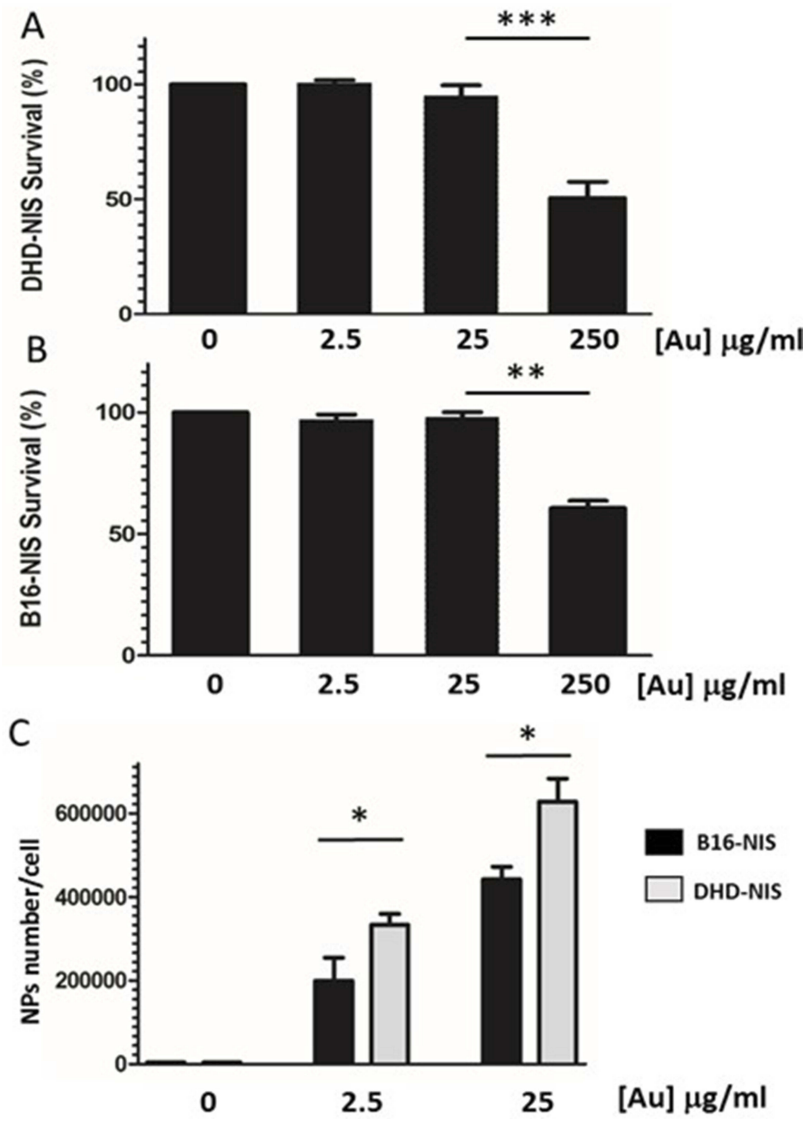

Figure 3 In vitro cytotoxicity and cellular uptake of PMAA-AuNPs nano-objects. Clonogenic assays were performed on DHD-NIS (**A**) or B16-NIS (**B**) cells treated for 2 hrs with PMAA-AuNPs nanoparticles at the indicated concentrations, before being washed and cultured for 9 to 14 days, respectively. The data presented are the mean±SEM of triplicates and are representative of three independent experiments. *p<0.05, **p<0.01, ***p<0.001. (**C**) Analysis of Au content per cell was conducted using a quadrupole ICP mass spectrometer, operated in standard mode. (*) indicates a significant difference observed in the Au uptake between the two cell types following exposure to the indicated concentrations of PMAA-AuNPs as determined by Student's *t* test.

The effect of different concentrations of PMAA-AuNPs in combination with ^{131}I was tested.

Figure 4A and B shows that the sensitization enhancement factor of PMAA-AuNPs increases with their concentration (2.5; 25 and 250 µg/mL [Au]). This effect is only detectable when radioiodine is taken up by the tumor cells, but not upon perchlorate treatment that prevents ^{131}I entry into the cells. Although detectable on both cell lines, no significant sensitizing effect at the lowest concentration of 2.5 µg/mL [Au] was measured. In contrast, 25 µg/mL [Au] could reduce the cell survival fraction from 82% to 48% for the DHD-NIS cells (Figure 4A) and from 90% to 57% for the B16-NIS cells (Figure 4B).

Assessment Of Radiosensitizing Potential Of PMAA-AuNPs To ^{131}I In Vivo

Our in vitro data led us to investigate the radiosensitizing potential of PMAA-AuNPs on NIS-expressing melanoma tumors. B16-NIS tumors were generated on the flank of Balb/c mice and their uptake ability was assessed by in vivo MicroSPECT/CT imaging using pertechnetate $^{99m}TcO_4$, the iodine substitute as a radiotracer (Figure 5). As expected, in

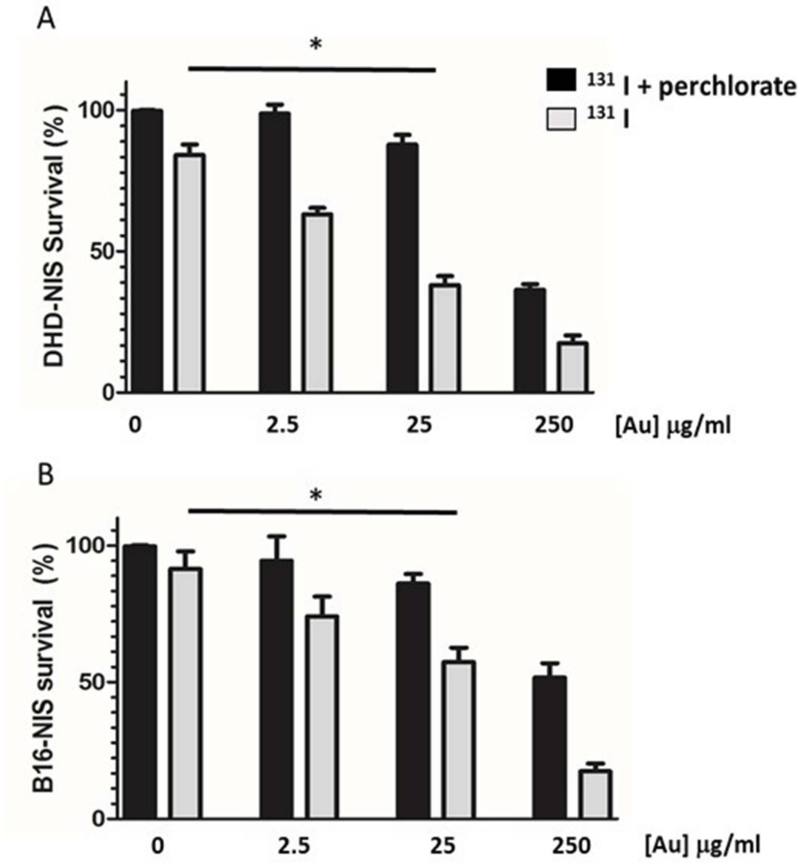

Figure 4 Radiosensitizing potential of PMAA-AuNPs to ^{131}I on B16-NIS and DHD-NIS cells. Clonogenic assays were performed on DHD-NIS (**A**) or B16-NIS (**B**) cells treated for 2 hrs with PMAA-AuNPs nanoparticles at the indicated concentrations, before being washed and exposed to ^{131}I alone (grey bars) (0.1 MBq for DHD-NIS cells, 0.2 MBq for B16-NIS cells) or to ^{131}I in association with sodium perchlorate (black bars). The data presented are the mean±SEM of triplicates and are representative of three independent experiments. *p<0.05.

control mice, significant radiotracer uptake was observed in tissues which express endogenous NIS, including the thyroid and stomach, and also the urinary bladder due to renal elimination (Figure 5A). In tumor-bearing mice (Figure 5B and C), comparable high levels of pertechnetate activity in the B16-NIS tumors were measured from day 4 after implantation, thus confirming the ability of the tumors to uptake the analog of radioiodine. Upon observation at the cellular level, immunohistochemistry on tissue sections of the B16-NIS tumors using anti-NIS antibodies indicated high heterogeneity in the NIS staining (Figure 5E) within the highly proliferating tumor cells (Figure 5D).

Therapy combining gold nanoparticles and radioiodine was then assessed. Established tumors were defined as reaching a volume averaging 100 mm^3, at which point, animals were randomly assigned to one of 4 treatment groups: saline (control), PMAA-AuNPs, ^{131}I, and PMAA-AuNPs/^{131}I. The nanoparticles were delivered by 3 intratumoral injections at day 6 after tumor implantation and ^{131}I treatment was injected i.p. (22 MBq) on day 7. Tumor progression was then measured over time and compared between the four groups (Figure 6A).

Figure 6A shows that control and PMAA-AuNPs tumors grew up to approximately 500 mm^3 within 12 days after implantation. Histologic analysis of the tumors shows highly proliferative cancer cells in the control tumors (Figure 7). Despite PMAA-AuNPs cytotoxicity observed in vitro, treatment alone at 1 mg/mL had a minimal impact on tumor growth and the nanoparticle-injected burdens fail to show any remarkable change/feature compared to that of the untreated group. The systemic treatment with 22 MBq ^{131}I by day 7 significantly impaired tumor progression resulting in a 15% reduction in the tumor volume by day 12 (439 mm^3 in the ^{131}I group vs 515 mm^3, in the control group, p<0.05). The smaller lesions observed in the radioiodine-treated mice featured few necrotic tumor cells throughout the lesions (25 necrotic cells/field in the ^{131}I group vs 11 in the control groups, p<0.05, Figure 7A–C). In agreement with the radiosensitizing effects observed in vitro, the combination of

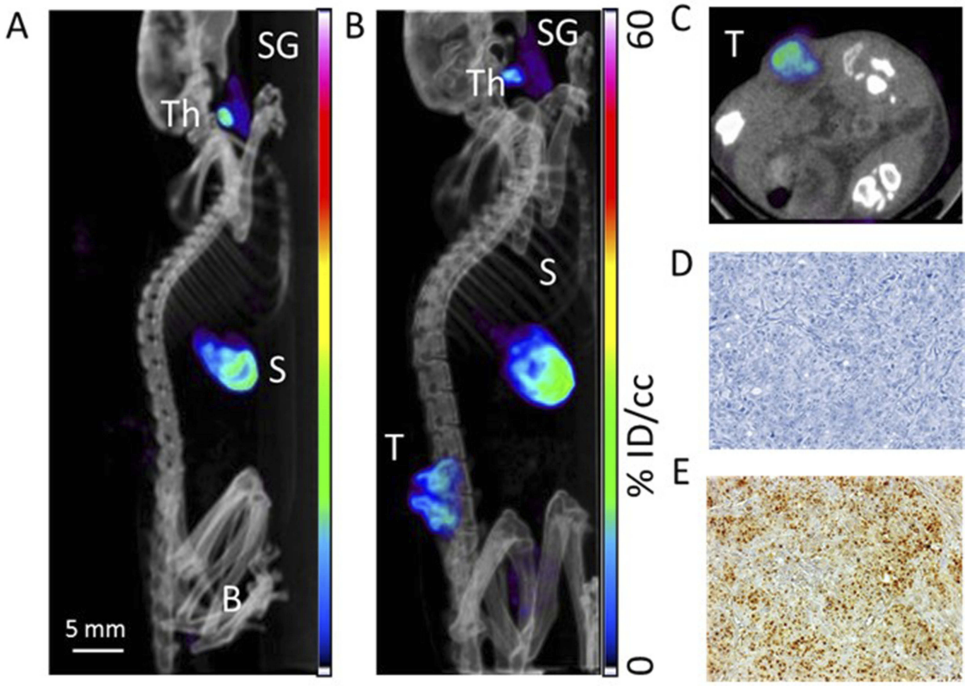

Figure 5 Assessment of radioiodine uptake by the NIS-expressing xenografts using microSPECT-CT imaging. (**A**) Radiotracer uptake was observed in tissues which express endogenous NIS in a control Balb/c female athymic mouse injected with an intraperitoneal administration of 15 MBq $^{99m}TcO_4$- and imaged with a microSPECT-CT camera (eXplore speCZT, General Electric): thyroid (Th), salivary glands (SG), stomach (S), and urinary bladder (B). Representative SPECT/CT sagittal (**B**) and transverse (**C**) sections of three-dimensional images of a B16-NIS-bearing mouse 10 days after subcutaneous injection of the tumour cells. (T) B16-NIS tumor. (**D**) Hematoxylin-stained sections of B16-NIS tumors show highly proliferating cells. (**E**) Representative NIS staining of tumor sections shows heterogeneity in NIS expression levels within lesions.

hybrid nanoparticles and ^{131}I attenuated tumor growth by 43% (291 mm^3 in the PMAA-AuNPs/^{131}I group vs 515 mm^3 in the control group, $p<0.001$) (Figure 6A) and by approximately 30% over radioiodine treatment alone (291 mm^3 in the PMAA-AuNPs/^{131}I group vs 439 mm^3 in the ^{131}I group, $p< 0.001$). Such reduction in tumor size was also reflected in the lighter weight of the burdens isolated from the mice treated with the combination therapy (Figure 6B and C). The most remarkable observation on the lesions treated with PMAA-AuNPs/^{131}I was the presence of much larger areas of necrosis that extended deep into the core of the lesions (Figure 7D). The number of necrotic cells per field exhibited a 4-fold increase in the PMAA-AuNPs/^{131}I-treated lesions compared to radioiodine alone ($p<0.01$, Figure 7D).

Discussion

Clinical trials are ongoing following convincing experimental evidence of the radio-enhancing potential of metallic nanoparticles in conventional RT where radiation beams are delivered to cancer cells from outside the body. Gold, platinum, and gadolinium are amongst the most investigated elements.[44] In contrast, the development of nanomedicine-based therapies to enhance the efficacy of internal RT, where the source of radiation comes from the radioisotope systemically injected into a patient, is far less advanced. β-particles emitters, among which ^{131}I is one of the most common radioisotopes, are the most widely used for cancer therapy.[45] However, radioiodine refractoriness hampers the therapy and nanoparticle-based radio-enhancing strategies easily translatable to the clinic are not available yet. The present study aimed at assessing the ability of radiosensitizing the neoplasm through the use of simple and reliable nanotherapeutics to be administered in combination with the standard systemic radioiodine therapy, with a perspective on clinical translation.

Gold nanoparticles (AuNPs) were chosen based on their ability to strongly interact with incident radiation and to increase the dose deposited close to the nano-object.[46] According to the recently described direct influence of the core size on the radiosensitizing properties of nano-objects,[47] we set up a protocol ensuring reproducibility of the gold core size. To improve their stability, cellular internalization and biocompatibility for in vivo application, PMAA chains have been grafted onto the

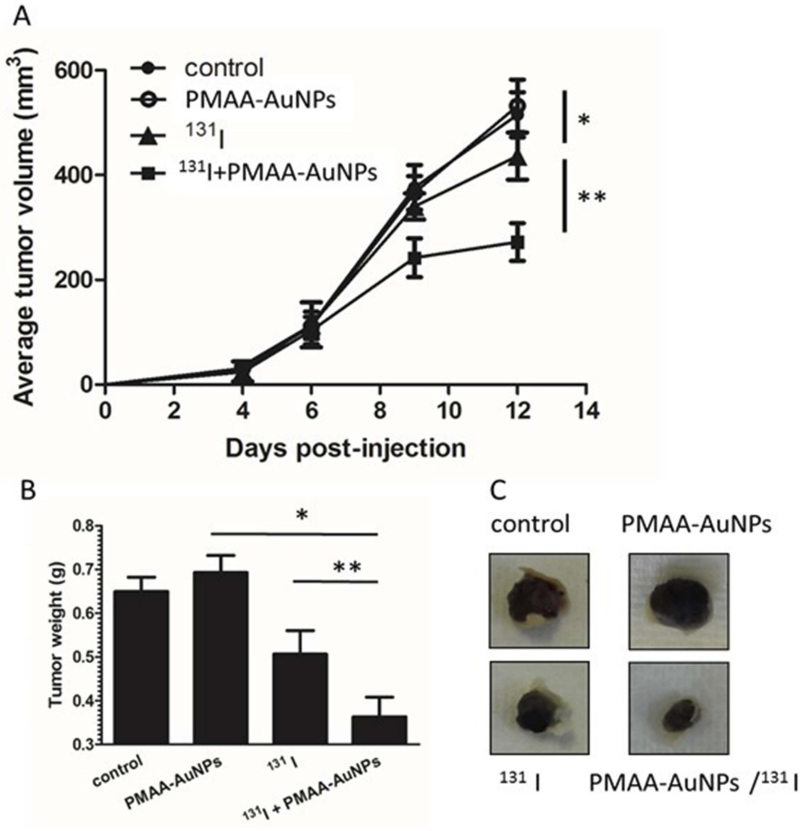

Figure 6 Assessment of radiosensitizing potential of PMAA-AuNPs to ^{131}I in vivo. (**A**) Tumor development was monitored over time in mice untreated (filled circles) or treated with either PMAA-AuNPs alone (open circles), or with an intraperitoneal injection of 22 MBq 131 I (filled triangles), or with a combination of Au-PMAA/^{131} I (filled squares). (**B**) Tumor weight was evaluated at necropsy. (**C**) Representative photographs of tumor xenografts from mice treated with PMAA-AuNPs, with radioiodine, or with PMAA-AuNPs/radioiodine. (n=5 mice/condition). *p<0.05; **p<0.001.

metallic core according to a direct method using polymer ligands obtained by controlled radical polymerization.[33] Among the key properties previously described by our group, such hybrid PMAA-AuNPs nanoparticles proved to safely withstand irradiation doses higher than 300 Gy, which is the maximum dose achieved in radioiodine treatment.[35]

Our in vitro data demonstrated the ability of PMAA-AuNPs to greatly increase the killing efficacy of iodine-131 on two types of tumor cells genetically modified in order to express the NIS symporter and to uptake iodine. Interestingly, this effect was obtained at a rather low radioactivity dose, at which free ^{131}I appeared to be essentially ineffective on NIS-expressing tumor cells. Comparatively, a stronger radiosensitizing effect was observed in the colorectal cancer DHD-NIS cells compared to the melanoma B16-NIS cells. Consistent with such effect, quantitative analyses indicated that, at the concentration of 25 μg/mL of PMAA-AuNPs, 27% more Au was detected in the DHD-NIS cells compared to the B16-NIS cells. In addition, both tumor cell types exhibited distinct intrinsic cellular radio-sensitivities, as the 50% lethal dose was reached with 32% less iodine-131 for DHD-NIS cells than for B16-NIS cells.

Encouraged by the in vitro performance of PMAA-AuNPs/^{131}I, we further explored the potential of the nano-objects to potentiate the efficacy of radioiodine systemically administered into B16-NIS-bearing mice. As a monotherapy administered on day 7 after tumor implantation into mice, iodine-131 was able to reduce tumor growth by 15%, indicating the tumor-inhibiting efficacy of radiation. Comparatively, the enrichment of tumors with PMAA-AuNPs prior to ^{131}I therapy led to a much more effective tumor growth inhibition. Nanoparticles-treated lesions were reduced by 50% in volume compared to control tumors and had significant lighter weight (reduced by 42%) after a single administration of 131-I. This boost in the killing efficacy of iodine-mediated radiations by PMAA-AuNPs was further evidenced by the much larger areas of necrotic cells observed in the treated tumors.

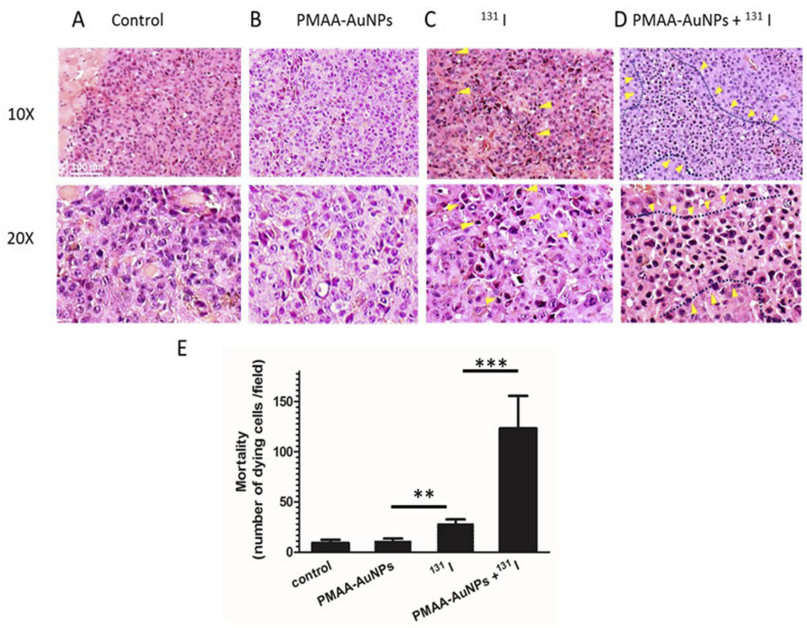

Figure 7 Histology of B16-NIS tumors after treatment with radioiodine combined or not with PMAA-AuNPs nanoparticles. Tumor histology was compared on sections (10× and 20× magnification) of lesions from B16-NIS challenged mice either untreated (**A**), or treated with PMAA-AuNPs (**B**), or with 20 MBq ^{131} I (**C**), or with PMAA-AuNPs/radioiodine (**D**). Arrows indicate the presence of pyknotic cells within lesions. (**E**) Numeration of the dying cells within lesions indicates a significantly increased mortality of the tumour cells in the PMAA-AuNPs/^{131}I treated-lesions compared to all other groups of treatments. **p<0.001, ***p<0.0001.

Three different phenomenon may account for the overall radio-enhancement effect observed on tumor models. The first mechanism of dose enhancement by PMAA-AuNPs results from the ability of gold atoms to absorb the gamma-radiation from ^{131}I uptaken by the NIS-expressing tumor cells and to generate secondary electrons enhancing cellular damage.[46] This mechanism is similar to that reported when high-Z element agents are used to sensitize EBRT by absorbing X-rays, or when such nanomaterials are directly labeled with radioisotopes in internal radioisotope RT. In the latter case, nanoparticles and radioisotopes are co-localized within tissues thus enabling a self-sensitization mechanism. In contrast, our study explored the possibility of applying the iodide-therapy and the nanoparticle separately. Once administered through the vasculature, radioiodine will reach the tumor cells and accumulate in the cytosol of the NIS-expressing tumor cells. For the cells that have internalized nanoparticles, the spatio-temporal co-localization with radiations will produce directly or indirectly high reactive species responsible for cellular damages directly lethal for the cells.

A second phenomenon may target the NIS-negative tumor cells that do not uptake radioiodine, but only nanoparticles. As shown by immunohistochemistry, B16-NIS tumors exhibited a marked heterogeneity in NIS expression. However, through the so-called "cross-fire" effect of radioiodine,[48] some electrons are emitted upon disintegration of ^{131}I within a few millimeters range and can therefore impact surrounding nanoparticle-enriched cells/tissues. This aspect is of high relevance for tumors exhibiting a high heterogeneity in radioisotope uptake. For patients with differentiated thyroid cancer (DTC), the efficacy of radio-iodide treatment is limited by the fact that metastases often display pronounced spatial non-uniformity.[49,50] Over time, patients develop progressive radioactive iodine-refractory DTC associated with a poor prognosis.[51,52] In this context, sensitizing the metastases with nanomedicine may help achieve more uniform coverage and overcome such resistance.

A third mechanism of radio-enhancement may stem from the interaction of gold and iodine atoms.[53,54] Indeed, a number of studies have reported the high reactivity of Au bulk surfaces and nanoparticles towards both iodine (I_2) and iodide (I) molecular ions. This chemisorption occurs spontaneously and increases the probability for one AuNP to be in the close vicinity to ^{131}I atoms, leading to an overall improvement of the radiosensitizing effect.

Beside thyroid cancer, radioiodide-based therapy has been explored in clinical trials for extra-thyroidal tumors after induction of NIS expression.[55] In this setting, the efficacy of the treatment is strictly dependent on the biological half-life of the radio-iodide in the body and on its

uptake by the target tumors, given that non-thyroidal cancer cells are not capable of prolonged iodide retention. Although major improvement of NIS gene-based therapy strategy has come from the use of vectors, replication-deficient, and oncolytic viruses,[19,56–59] the applicability of this approach to treat non-thyroidal neoplasms is still hampered by the reduced capacity of such tumors to accumulate ^{131}I.[19,20] Various strategies have been tested so far to improve this approach, with limited efficacy. Sensitizing the neoplasms through the use of metal-hybrid nano-agents may therefore offer a new opportunity to improve the strategy.

Beyond ^{131}I based-treatment, these results open up novel perspectives for using high-Z metallic NPs in molecular radiation therapy demonstrating heterogeneous dose distributions, including yttrium-90 treatment for liver tumors[60] or 153Sm-EDTMP in bone cancer.[61]

Finally, by those combined effects, nano-material-based radio-internal therapies may also help reducing the delivered dose and thus the radiotoxicity of the radiopharmaceutical to sound tissues and to the critical organs. As an example, off-target accumulation of radioiodine in cells of the salivary glands, or so-called sialoadenitis, is a common complication of ^{131}I therapy.[62] Moreover, the occurrence of leukaemia has been correlated with higher radioactive iodine doses.[63] Thus, it is tempting to speculate that protection of normal tissues against the cellular toxicity induced by beta particles via the use of radiosensitizing nanomaterial may mitigate side effects. This proof of concept paves the way to promising investigations using systemic administration of the particles in combination with ^{131}I therapy to address this point. In some patients, beta-particle therapy using ^{131}I is inadequate and another strategy is needed using more effective radionuclide targeting the sodium/iodide symporter (NIS). Astatine (^{211}At) is receiving increasing attention as an alpha-emitter for targeted radionuclide therapy.[64–66] Astatine is a halogen element with similar chemical properties to iodine. Alpha particles emitted from ^{211}At with a branching ratio of 41.8% (5.98MeV) has higher linear energy transfer as compared to beta particles from ^{131}I (0.97MeV) and exert a better therapeutic effect by inducing DNA double-strand breaks and free radical formation.[67] Future work will have to investigate this interesting possibility.

Given that such nano-objects are amenable to subsequent grafting on their carboxylic acid moieties, future perspectives can also expand towards motifs providing additional targeting ability (for thyroid tissues or other cancer markers). Additional applications of emerging "advanced materials" such as grafting chemotherapeutic drugs, photothermal effects, immunotherapy, etc. can also be envisaged for enhanced cancer treatment.

Conclusion

This work is the first to show the efficacy of a clinically relevant approach combining hybrid polymer-grafted nano-objects (PMAA-AuNPs) to systemic radioiodine therapy. This proof of principle expands the use of functionalized nanoparticles as radio-sensitizers to the field of internal radioisotope RT. These results open up novel perspectives for using high-Z metallic NPs in molecular radiation therapy, not only in ^{131}I-based treatment, but in additional radiopharmaceutical therapies demonstrating heterogeneous dose distributions.

Ethical Approval

All applicable international, national, and/or institutional guidelines for the care and use of animals were followed.

Acknowledgments

This work was supported by INSERM, the French National Research Agency (14IAS001MCSR) and by a grant from CEA (A-PTTOX-02-52-03). The authors thank the radiopharmaceutical team of the Centre Antoine Lacassagne (Nadine Sapin, Guy Martinico, Stéphane Espitallier, Didier Alberato) for their help with radioisotope production and handling. We thank the IRCAN Animal Core Facility for providing access to their equipment. The platform and expertise of the Electron Microscopy Facility of I2BC (Université Paris Sud, CEA-CNRS UMR 9198) is also acknowledged.

Disclosure

Miss Béatrice Cambien reports grants from TIRO laboratory, during the conduct of the study. All authors declare that they have no other conflicts of interest in this work.

References

1. Brown JM, Wilson WR. Exploiting tumour hypoxia in cancer treatment. *Nat Rev Cancer*. 2004;4(6):437–447. doi:10.1038/nrc1367
2. Steel GG, Peckham MJ. Exploitable mechanisms in combined radiotherapy-chemotherapy: the concept of additivity. *Int J Radiat Oncol Biol Phys*. 1979;5(1):85–91. doi:10.1016/0360-3016(79)90044-0
3. Touchefeu Y, Vassaux G, Harrington KJ. Oncolytic viruses in radiation oncology. *Radiother Oncol*. 2011;99(3):262–270. doi:10.1016/j.radonc.2011.05.078

4. Hickson I, Zhao Y, Richardson CJ, et al. Identification and characterization of a novel and specific inhibitor of the ataxia-telangiectasia mutated kinase ATM. *Cancer Res*. 2004;64(24):9152–9159.
5. Farmer H, McCabe N, Lord CJ, et al. Targeting the DNA repair defect in BRCA mutant cells as a therapeutic strategy. *Nature*. 2005;434(7035):917–921.
6. Zhao Y, Thomas HD, Batey MA, et al. Preclinical evaluation of a potent novel DNA-dependent protein kinase inhibitor NU7441. *Cancer Res*. 2006;66(10):5354–5362.
7. Hainfeld JF, Slatkin DN, Smilowitz HM. The use of gold nanoparticles to enhance radiotherapy in mice. *Phys Med Biol*. 2004;49(18):N309–315.
8. Chang MY, Shiau AL, Chen YH, Chang CJ, Chen HH, Wu CL. Increased apoptotic potential and dose-enhancing effect of gold nanoparticles in combination with single-dose clinical electron beams on tumor-bearing mice. *Cancer Sci*. 2008;99(7):1479–1484.
9. Butterworth KT, McMahon SJ, Currell FJ, Prise KM. Physical basis and biological mechanisms of gold nanoparticle radiosensitization. *Nanoscale*. 2012;4(16):4830–4838.
10. Taggart LE, McMahon SJ, Currell FJ, Prise KM, Butterworth KT. The role of mitochondrial function in gold nanoparticle mediated radiosensitisation. *Cancer Nanotechnol*. 2014;5(1):5. doi:10.1186/s12645-014-0005-7
11. Calugaru V, Magne N, Herault J, Bonvalot S, Le Tourneau C, Thariat J. [Nanoparticles and radiation therapy]. *Bull Cancer*. 2015;102(1):83–91. doi:10.1016/j.bulcan.2014.10.002
12. Wang Y, Liang R, Fang F. Applications of nanomaterials in radiotherapy for malignant tumors. *J Nanosci Nanotechnol*. 2015;15(8):5487–5500. doi:10.1166/jnn.2015.10617
13. Her S, Jaffray DA, Allen C. Gold nanoparticles for applications in cancer radiotherapy: mechanisms and recent advancements. *Adv Drug Deliv Rev*. 2017;109:84–101. doi:10.1016/j.addr.2015.12.012
14. Kunz-Schughart LA, Dubrovska A, Peitzsch C, et al. Nanoparticles for radiooncology: mission, vision, challenges. *Biomaterials*. 2017;120:155–184. doi:10.1016/j.biomaterials.2016.12.010
15. Kawashima H. Radioimmunotherapy: a specific treatment protocol for cancer by cytotoxic radioisotopes conjugated to antibodies. *Sci World J*. 2014;2014:492061. doi:10.1155/2014/492061
16. Haugen BR, Alexander EK, Bible KC, et al. 2015 American Thyroid Association Management Guidelines for Adult Patients with Thyroid Nodules and Differentiated Thyroid Cancer: the American Thyroid Association Guidelines Task Force on Thyroid Nodules and Differentiated Thyroid Cancer. *Thyroid*. 2016;26(1):1–133. doi:10.1089/thy.2015.0020
17. Merron A, Baril P, Martin-Duque P, et al. Assessment of the Na/I symporter as a reporter gene to visualize oncolytic adenovirus propagation in peritoneal tumours. *Eur J Nucl Med Mol Imaging*. 2010;37(7):1377–1385. doi:10.1007/s00259-009-1379-3
18. Xing M, Haugen BR, Schlumberger M. Progress in molecular-based management of differentiated thyroid cancer. *Lancet*. 2013;381(9871):1058–1069. doi:10.1016/S0140-6736(13)60109-9
19. Peerlinck I, Merron A, Baril P, et al. Targeted radionuclide therapy using a Wnt-targeted replicating adenovirus encoding the Na/I symporter. *Clin Cancer Res*. 2009;15(21):6595–6601. doi:10.1158/1078-0432.CCR-09-0262
20. Barton KN, Stricker H, Brown SL, et al. Phase I study of noninvasive imaging of adenovirus-mediated gene expression in the human prostate. *Mol Ther*. 2008;16(10):1761–1769. doi:10.1038/mt.2008.172
21. Zwarthoed C, Chatti K, Guglielmi J, et al. Single-Photon Emission Computed Tomography For Preclinical Assessment Of Thyroid Radioiodide Uptake Following Various Combinations Of Preparative Measures. *Thyroid*. 2016;26(11):1614–1622. doi:10.1089/thy.2015.0652
22. Lakshmanan A, Scarberry D, Green JA, Zhang X, Selmi-Ruby S, Jhiang SM. Modulation of thyroidal radioiodide uptake by oncological pipeline inhibitors and apigenin. *Oncotarget*. 2015;6(31):31792–31804. doi:10.18632/oncotarget.5172
23. Song X, Liang C, Feng L, Yang K, Liu Z. Iodine-131-labeled, transferrin-capped polypyrrole nanoparticles for tumor-targeted synergistic photothermal-radioisotope therapy. *Biomater Sci*. 2017;5(9):1828–1835. doi:10.1039/c7bm00409e
24. Tian L, Chen Q, Yi X, et al. Radionuclide I-131 labeled albumin-paclitaxel nanoparticles for synergistic combined chemo-radioisotope therapy of cancer. *Theranostics*. 2017;7(3):614–623. doi:10.7150/thno.17381
25. Zhao H, Chao Y, Liu J, et al. Polydopamine coated single-walled carbon nanotubes as a versatile platform with radionuclide labeling for multimodal tumor imaging and therapy. *Theranostics*. 2016;6(11):1833–1843. doi:10.7150/thno.16047
26. Chao Y, Wang G, Liang C, et al. Rhenium-188 labeled tungsten disulfide nanoflakes for self-sensitized, near-infrared enhanced radioisotope therapy. *Small*. 2016;12(29):3967–3975. doi:10.1002/smll.201601375
27. Chao Y, Liang C, Yang Y, et al. Highly effective radioisotope cancer therapy with a non-therapeutic isotope delivered and sensitized by nanoscale coordination polymers. *ACS Nano*. 2018. doi:10.1021/acsnano.8b02400
28. Dziawer L, Koźmiński P, Męczyńska-Wielgosz S, et al. Gold nanoparticle bioconjugates labelled with 211At for targeted alpha therapy. *RSC Adv*. 2017;7:1024–41032. doi:10.1039/C7RA06376H
29. Kucka J, Hruby M, Konak C, Kozempel J, Lebeda O. Astatination of nanoparticles containing silver as possible carriers of 211At. *Appl Radiat Isot*. 2006;64(2):201–206. doi:10.1016/j.apradiso.2005.07.021
30. Hua S, de Matos MBC, Metselaar JM, Storm G. Current trends and challenges in the clinical translation of nanoparticulate nanomedicines: pathways for translational development and commercialization. *Front Pharmacol*. 2018;9:790. doi:10.3389/fphar.2018.00790
31. Ngwa W, Korideck H, Kassis AI, et al. In vitro radiosensitization by gold nanoparticles during continuous low-dose-rate gamma irradiation with I-125 brachytherapy seeds. *Nanomedicine*. 2013;9(1):25–27.
32. Rausch K, Reuter A, Fischer K, Schmidt M. Evaluation of nanoparticle aggregation in human blood serum. *Biomacromolecules*. 2010;11(11):2836–2839.
33. Le Goas MP, Paquirissamy A, Gargouri D, et al. Irradiation effects on polymer-grafted gold nanoparticles for cancer therapy. *ACS Appl Bio Mater*. 2018;2(1):144–154. doi:10.1021/acsabm.8b00484
34. Rinkenauer AC, Press AT, Raasch M, et al. Comparison of the uptake of methacrylate-based nanoparticles in static and dynamic in vitro systems as well as in vivo. *J Control Release*. 2015;216:158–168.
35. Maxon HR 3rd, Englaro EE, Thomas SR, et al. Radioiodine-131 therapy for well-differentiated thyroid cancer–a quantitative radiation dosimetric approach: outcome and validation in 85 patients. *J Nucl Med*. 1992;33(6):1132–1136.
36. Perron B, Rodriguez AM, Leblanc G, Pourcher T. Cloning of the mouse sodium iodide symporter and its expression in the mammary gland and other tissues. *J Endocrinol*. 2001;170(1):185–196.
37. Richard-Fiardo P, Franken PR, Lamit A, et al. Normalisation to blood activity is required for the accurate quantification of Na/I symporter ectopic expression by SPECT/CT in individual subjects. *PLoS One*. 2012;7(3):e34086.
38. Vassaux G, Zwarthoed C, Signetti L, et al. Iodinated contrast agents perturb iodide uptake by the thyroid independently of free iodide. *J Nucl Med*. 2018;59(1):121–126.
39. Huc-Brandt S, Marcellin D, Graslin F, et al. Characterisation of the purified human sodium/iodide symporter reveals that the protein is mainly present in a dimeric form and permits the detailed study of a native C-terminal fragment. *Biochim Biophys Acta*. 2011;1808(1):65–77.
40. Cambien B, Franken PR, Lamit A, et al. (9)(9)mTcO(4)–, auger-mediated thyroid stunning: dosimetric requirements and associated molecular events. *PLoS One*. 2014;9(3):e92729.
41. Loening AM, Gambhir SS. AMIDE: a free software tool for multimodality medical image analysis. *Mol Imaging*. 2003;2(3):131–137.
42. Wang Z, Tan B, Hussain I, et al. Design of polymeric stabilizers for size-controlled synthesis of monodisperse gold nanoparticles in water. *Langmuir*. 2007;23(2):885–895.

43. Kelly KL, Coronado E, Zhao LL, Schatz GC. The optical properties of metal nanoparticles: the influence of size, shape, and dielectric environment. *J Phys Chem*. 2003;B 107:668–677.
44. Muddineti OS, Ghosh B, Biswas S. Current trends in using polymer coated gold nanoparticles for cancer therapy. *Int J Pharm*. 2015;484 (1–2):252–267.
45. Zhang L, Chen H, Wang L, et al. Delivery of therapeutic radioisotopes using nanoparticle platforms: potential benefit in systemic radiation therapy. *Nanotechnol Sci Appl*. 2010;3:159–170.
46. Rosa S, Connolly C, Schettino G, Butterworth KT, Prise KM. Biological mechanisms of gold nanoparticle radiosensitization. *Cancer Nanotechnol*. 2017;8(1):2.
47. Khalil TT, Bazzi R, Roux S, Fromm M. The contribution of hydrogen peroxide to the radiosensitizing effect of gold nanoparticles. *Colloids Surf B Biointerfaces*. 2019;175:606–613.
48. Hamoudeh M, Kamleh MA, Diab R, Fessi H. Radionuclides delivery systems for nuclear imaging and radiotherapy of cancer. *Adv Drug Deliv Rev*. 2008;60(12):1329–1346.
49. Dorn R, Kopp J, Vogt H, Heidenreich P, Carroll RG, Gulec SA. Dosimetry-guided radioactive iodine treatment in patients with metastatic differentiated thyroid cancer: largest safe dose using a risk-adapted approach. *J Nucl Med*. 2003;44(3):451–456.
50. Jentzen W, Verschure F, van Zon A, et al. 124I PET assessment of response of bone metastases to initial radioiodine treatment of differentiated thyroid cancer. *J Nucl Med*. 2016;57(10):1499–1504.
51. Mirallie E, Guillan T, Bridji B, et al. Therapeutic impact of 18FDG-PET/CT in the management of iodine-negative recurrence of differentiated thyroid carcinoma. *Surgery*. 2007;142(6):952–958; discussion 952–958.
52. Makeieff M, Burcia V, Raingeard I, et al. Positron emission tomography-computed tomography evaluation for recurrent differentiated thyroid carcinoma. *Eur Ann Otorhinolaryngol Head Neck Dis*. 2012;129(5):251–256.
53. Cheng W, Dong S, Wang E. Iodine-induced gold-nanoparticle fusion/fragmentation/aggregation and iodine-linked nanostructured assemblies on a glass substrate. *Angew Chem Int Ed Engl*. 2003;42 (4):449–452.
54. Figuerola A, Franchini IR, Fiore A, et al. End-to-end assembly of shape-controlled nanocrystals via a nanowelding approach mediated by gold domains. *Adv Mater*. 2009;21(5):550–554.
55. Micali S, Bulotta S, Puppin C, et al. Sodium iodide symporter (NIS) in extrathyroidal malignancies: focus on breast and urological cancer. *BMC Cancer*. 2014;14:303.
56. Chisholm EJ, Vassaux G, Martin-Duque P, et al. Cancer-specific transgene expression mediated by systemic injection of nanoparticles. *Cancer Res*. 2009;69(6):2655–2662.
57. Richard-Fiardo P, Hervouet C, Marsault R, et al. Evaluation of tetrafunctional block copolymers as synthetic vectors for lung gene transfer. *Biomaterials*. 2015;45:10–17.
58. Hingorani M, White CL, Zaidi S, et al. Radiation-mediated up-regulation of gene expression from replication-defective adenoviral vectors: implications for sodium iodide symporter gene therapy. *Clin Cancer Res*. 2008;14(15):4915–4924.
59. Naik S, Galyon GD, Jenks NJ, et al. Comparative oncology evaluation of intravenous recombinant oncolytic vesicular stomatitis virus therapy in spontaneous canine cancer. *Mol Cancer Ther*. 2018;17 (1):316–326.
60. Kennedy AS, Nutting C, Coldwell D, Gaiser J, Drachenberg C. Pathologic response and microdosimetry of (90)Y microspheres in man: review of four explanted whole livers. *Int J Radiat Oncol Biol Phys*. 2004;60(5):1552–1563.
61. Hobbs RF, McNutt T, Baechler S, et al. A treatment planning method for sequentially combining radiopharmaceutical therapy and external radiation therapy. *Int J Radiat Oncol Biol Phys*. 2011;80(4):1256–1262.
62. Van Nostrand D. Sialoadenitis secondary to (1)(3)(1)I therapy for well-differentiated thyroid cancer. *Oral Dis*. 2011;17(2):154–161.
63. Van Nostrand D, Neutze J, Atkins F. Side effects of "rational dose" iodine-131 therapy for metastatic well-differentiated thyroid carcinoma. *J Nucl Med*. 1986;27(10):1519–1527.
64. Ogawa K, Mizuno Y, Washiyama K, et al. Preparation and evaluation of an astatine-211-labeled sigma receptor ligand for alpha radionuclide therapy. *Nucl Med Biol*. 2015;42(11):875–879.
65. Ohshima Y, Sudo H, Watanabe S, et al. Antitumor effects of radionuclide treatment using alpha-emitting meta-(211)At-astato-benzylguanidine in a PC12 pheochromocytoma model. *Eur J Nucl Med Mol Imaging*. 2018;45(6):999–1010.
66. Li HK, Morokoshi Y, Nagatsu K, Kamada T, Hasegawa S. Locoregional therapy with alpha-emitting trastuzumab against peritoneal metastasis of human epidermal growth factor receptor 2-positive gastric cancer in mice. *Cancer Sci*. 2017;108(8):1648–1656.
67. Andersson H, Palm S, Lindegren S, et al. Comparison of the therapeutic efficacy of 211At- and 131I-labelled monoclonal antibody MOv18 in nude mice with intraperitoneal growth of human ovarian cancer. *Anticancer Res*. 2001;21(1A):409–412.